European Polymer Journal 94 (2017) 43–55

Contents lists available at ScienceDirect

European Polymer Journal

journal homepage: www.elsevier.com/locate/europolj

Macromolecular Nanotechnology

Magnetic composite films based on alginate and nano-iron oxide particles obtained by synthesis "in situ"

Gianina A. Kloster[a], Diego Muraca[b,c], Mirna A. Mosiewicki[a], Norma E. Marcovich[a,*]

[a] Instituto de Investigaciones en Ciencia y Tecnología de Materiales (INTEMA-CONICET), Juan B. Justo 4302, Mar del Plata, Buenos Aires 7600, Argentina

[b] Laboratório Nacional de Nanotecnologia (LNNano), Centro Nacional de Pesquisa em Energia e Materiais (CNPEM), CEP 13083-970 Campinas, São Paulo, Brazil

[c] Instituto de Física 'Gleb Wataghin', Universidade Estadual de Campinas (UNICAMP), CEP13083-859 Campinas, São Paulo, Brazil

ARTICLE INFO

Keywords:
Magnetic nanocomposites
Iron oxide nanoparticles
Alginate films

ABSTRACT

In this work, sodium alginate was used as the polymeric matrix of magnetic nanocomposite films where iron oxide particles, in percentages varying from 2 to 10 wt.% (respect to alginate content), were synthesized "in situ". The effects of the nanoparticle concentration and the addition of 30 wt.% of glycerol as plasticizer on the properties of the composite films were analyzed by X-ray diffraction, scanning electron microscopy, infrared spectroscopy, tensile tests, zero field cooling/field cooling measurements and isothermal magnetization as function of applied fields at different temperatures. The presence of residual salts formed during the synthesis process, the film microstructure and the interactions developed between magnetic particles and between particles and matrix were the most important factors that affected the film properties. All the synthesized composite films showed super paramagnetic behavior, while the recorded blocking and irreversibility temperatures were lower for the plasticized ones, indicating that the size of the magnetic particles/particle agglomerates formed in these samples was smaller and the particle dispersion in the polymeric matrix better than those obtained in films prepared without glycerol.

1. Introduction

The use of magnetic polymeric nanocomposites for the remediation of wastewater and soil has been studied with a lot of interest in the last years because of the special advantages obtained from the combination of these two types of materials. If the polymer is biodegradable, the benefits are even greater because at the end of the useful life of the material, it does not cause posterior pollution. The presence of a magnetic phase or component offers important new properties to the composite: i.e. during an adsorption process the adsorbent material is in contact the aqueous solution to be purified but after that, it could be difficult to separate both phases and consequently the adsorbent could not be recovered to be used again. In order to solve this problem, separation technologies employing magnetic adsorbents are an alternative method for treating water/wastewater that has received considerable attention in recent years [1].

Among a variety of biopolymers, alginate presents a combination of abundant and attractive features such as low-cost, biodegradability, biocompatibility [2], renewability, and excellent binding ability [3]. It is a linear copolymer composed of (1–4)-linked β-D-mannuronic acid (M) and its C-5 epimer α-L-guluronic acid (G) [4] arranged in a block-wise fashion, constructed not only of homopolyuronate blocks (MM or GG) but also of alternating blocks (MG). This natural-occurring polyelectrolytic polysaccharide is found in

* Corresponding author.
E-mail address: marcovic@fi.mdp.edu.ar (N.E. Marcovich).

http://dx.doi.org/10.1016/j.eurpolymj.2017.06.041
Received 4 April 2017; Received in revised form 21 June 2017; Accepted 25 June 2017
Available online 27 June 2017

all species of brown algae and some species of bacteria [5,6]. It has a large number of fields of applications, including medicine, agriculture, drug carrying and release and packaging fields including encapsulation of herbicides, microorganisms and cells [7]. Other of their interesting uses is for the adsorption of certain types of heavy metal ions and dyes in wastewater [3]. Specifically in the case of alginate, the presence of the carboxyl groups gives this biopolymer the ability to form complex with variety of multivalent ions. In aqueous solution (at pH $>$ 3.4), alginate is negatively charged, due to the prevalence of carboxyl groups in both G and M subunits, where the carboxyl groups become deprotonated except at very low pH. The use of alginate as exchanger for heavy metal ion has been tested in many metals such as Co, Cu, Cd and Zn [8–11].

On the other hand, using iron oxides like magnetite, hematite and maghemite as reinforcements for the polymeric matrices, the resultant composite would incorporate new and interesting characteristics. If single domain iron oxides particles are below a critical size, super-paramagnetic behavior could be observed, which means that the particles, even embedded in a polymeric matrix, can be oriented in the direction of the applied magnetic field like paramagnets, but with a much larger susceptibility. Thus, the size of the particles has special interest because it will determine if the particles are on the super-paramargentic regime or not (i.e. it can provide a sudden spatial magnetization in front of a magnetic field when they are on the super-paramagnetic regime). Iron oxides particles at room temperature tend to behave like super-paramagnetic materials if their size is below 15 nm [12].

In order to incorporate magnetite nanoparticles into different polymeric matrix or environments, the way of synthesis is very important since it affects their final magnetic properties. For example, one of the more reported difficulties during the synthesis of this type of material is to avoid the agglomeration of nanoparticles when they are synthesized prior to being included within the matrix. The in situ co-precipitation of magnetic nanoparticles seems to avoid the formation of large agglomerates. Also, electrostatic repulsion between the nanoparticles makes them stable and prevents the aggregation. Pardoe et al. [13] investigated the magnetic properties of magnetite and maghemite particles synthesized in the presence of dextran or polyvinyl alcohol and verified that superparamagnetic blocking temperature depends on the polymer nature. Moreover, different attempts of synthesis of iron oxide nanoparticles/alginate systems have been proposed [5,14–16]. Some of the methods involve the gelation of alginate and ferrous ion, the precipitation of ferrous hydroxide by the alkaline treatment of alginate and the oxidation of ferrous hydroxide with an oxidizing agent. Any of these methods have their own difficulties, and usually results in a nonmagnetic form of iron oxide. Ma et al. [6] proposed a two-step co-precipitation method that involved the synthesis of magnetite from Fe^{+2} and Fe^{+3} in alkaline solution and then the combination of the particles obtained with alginate by dispersion using ultrasonication. Mohammadi et al. [17] prepared superparamagnetic sodium alginate-coated Fe_3O_4 nanoparticles as a novel magnetic adsorbent, by in situ co-precipitation method, in which Fe_3O_4 nanoparticles were precipitated from $FeCl_3$ and $FeCl_2$ under alkaline medium in the presence of sodium alginate. They suggested that the alginate coating of nanoparticles could be due electrostatic attraction between carboxylate groups of sodium alginate and Fe^{2+} and Fe^{3+} ions of Fe_3O_4 nanoparticles.

The interactions between alginate and iron oxides have been studied and found to be pH dependant [2]. The isoelectric point of Fe_3O_4 nanoparticles was around 6.85 [2,18]. At pH below isoelectric point, the Fe_3O_4 nanoparticles surfaces are positively charged due to the formation of $–FeOH_2^+$ groups, while at pH above isoelectric point, they are negatively charged due to the formation of FeO^- groups [19].

We have already studied the synthesis of chitosan-nanomagnetite composite films using an in situ co-precipitation method [20]. In the present work, we propose to adjust this simple one step co-precipitation technique to prepare alginate nanocomposite films with various concentrations of iron oxide nanoparticles. The effect of magnetic nanoparticles concentration on their physical, chemical and mechanical properties, and especially on their magnetic response is presented.

2. Experimental

2.1. Materials

Sodium alginate (SA) in powder form supplied by Sigma Aldrich (moisture content $\leq$ 14.1%; viscosity (1% in water) = 19 cps; pH (1% in water) = 7.6) was used as received. Glycerol (gly) purchased from DEM Mar del Plata was used as plasticizer. Ferric chloride ($FeCl_3{\cdot}6H_2O$), ferrous sulphate ($FeSO_4{\cdot}7H_2O$) and sodium hydroxide were purchased from Aldrich.

2.2. Methods

2.2.1. Preparation of composite films

The films were prepared by casting. Alginate solution (2 w/v%) was prepared by incorporating alginate powder in an aqueous sodium hydroxide solution (0.3 mol/L) and applying magnetic stirring during 1.5 h. Glycerol, in a 30 wt.% respect to the alginate mass was also added to the solution when applicable. A 0.2 mol/L aqueous iron salt solution was made using a molar ratio of Fe^{2+}:Fe^{3+} = 1:2. The alginate and iron salts solutions were mixed in the appropriate proportions to obtain films with 0, 2, 5, 7 and 10 nominal wt.% of magnetic nanoparticles (MNP) (calculated with respect to the mass of alginate). The resulting suspensions were poured into Petri dishes (diameter = 14 cm) and dried in a convective oven at 40 °C. The obtained films (thicknesses ~100–150 μm) were kept in a closed container containing dried silica gel at room temperature (23 ± 2 °C) until testing.

2.2.2. Characterization of composite films

2.2.2.1. Infrared spectroscopy characterization. FTIR spectra were obtained in transmission mode from samples in KBr pellets over the range of 4000–600 cm^{-1} using a Thermo Scientific Nicolet 6700 Fourier transform infrared spectrometer. Films were previously

grounded using liquid nitrogen and then mixed with KBr to prepare the testing samples. The spectra were recorded with a resolution of 2 cm^{-1} and averaged over 32 scans.

2.2.2.2. X-ray diffraction. The crystal structure of the nanocomposites was characterized by X-ray powder diffraction (XRD), using Cu Kα radiation (λ = 1.5418 Å), using a PANalytical X'Pert Pro diffractometer operated at 40 kv, 300 mA and 0.6°/min.

2.2.2.3. Transmission electron microscopy. Microscopy analysis was performed on a TEM-FEG (JEM 2100F) field-emission gun transmission electron microscope (voltage: 200 kV, spot size 3). The images were acquired using a Gatan, Orius SC600/831 camera at different resolutions. To prepare the test samples first a selected nanocomposite film was dissolved in distilled water, leading to the precipitation of the nanoparticles that were then separated from the solution by centrifugation. These particles were subsequently intensively washed with distilled water in order to eliminate most of the remaining polymer and finally dried by liophilization. Then, the particles were dispersed in milli-q water and sonicated during 15 min. The samples for microscopy observation were prepared by drying a drop of this last nanoparticle suspension during 24 h at room temperature on a Ted Pella ultrathin cooper film on a holey carbon. The obtained images were analyzed using ImageJ free software.

2.2.2.4. Scanning electron microscopy. Selected cross sections (obtained by cryo-fracture after immersing samples in liquid air) of the films were examined using a scanning electron microscope (JEOL, model JSM-6460 LV). The pieces of the films were mounted on bronze stubs using a double-sided tape and then coated with gold, before being observed under the microscope.

2.2.2.5. Mechanical characterization. Tensile tests were performed at room temperature (23 ± 2 °C) using an Instron Universal Testing Machine model 8501. At least four specimens from each film (strips of 5 × 25 mm) were tested. Crosshead speed was set at 10 mm/min. The ultimate strength (σ_u), elongation at break (ε_u) and elastic modulus (E) were calculated as described in ASTM D638-94b (1994). Prior to running mechanical tests, films were conditioned for 72 h at 65 ± 5% relative humidity (RH) at room temperature.

2.2.2.6. Magnetic characterization. The magnetic properties of the composites were obtained using a commercial SQUID magnetometer (Quantum Design, MPMS XL). Both isothermal magnetization curves as well as Zero Field Cooling/Field Cooling (ZFC/FC) measurements were performed in order to characterize the magnetic properties of the nanocomposite films. The ZFC/FC cooling measurement protocol was carried out as follows: the sample was first cooled down from 300 to 5 K in zero magnetic field. Then, a static magnetic field at 50 Oe was applied and the magnetization was measured while increasing the temperature up to 300 K. Subsequently, the sample was cooled down to 5 K under the same applied magnetic field (50 Oe) and the magnetization was measured while warming up the sample from 5 to 300 K. Also, isothermal measurements were carried out at different temperatures between 2 and 300 K.

3. Results and discussion

3.1. Physical, chemical and mechanical properties of the nanocomposite films

Photographs of the plasticized films are shown in Fig. 1. It is clear that with the increase of the content of iron oxide, the films become darker. In addition, the visual observation of the films surfaces allowed us to detect a white solid, which is probably barely visible in the pictures, that could correspond to salts (NaCl, Na_2SO_4) formed by combination of the Na^+ coming from the sodium hydroxide used in the synthesis of the films as precipitating agent for iron oxides, and the Cl^- and SO_4^{2-} coming from the ferric and ferrous salts. From the images it also can be noticed that the flexibility of the films does not change very much (i.e. no cracks or fissures created during drying or demolding are noticed) as the iron oxide content increases. The non-plasticized films present a similar appearance.

FTIR spectra of selected films are shown in Fig. 2. The presence of the iron oxide in the composite samples should be observed in the region of 700–500 cm^{-1} [21,22], as two absorption bands at about 636 and 592 cm^{-1} [23,25], which could be attributed to the Fe—O vibrations in octahedral and tetrahedral sites [2,23–25]. However in our case only a slightly increased intensity in the zone about 620 cm^{-1} is noticed for samples containing MNP (respect to the spectra of the neat matrices), which cannot provide enough

Fig. 1. Plasticized nanocomposite films. From left to right: 0, 2, 5, 7 and 10 wt.% MNP concentration.

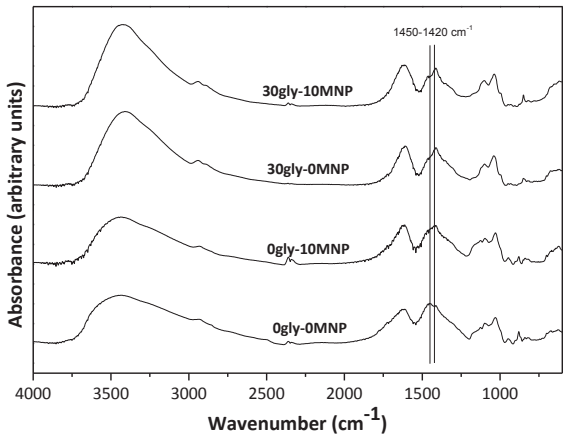

Fig. 2. FTIR spectra of films without glycerol and with 30 wt.% of glycerol and 0 or 10 wt.% MNP.

evidence about the successful incorporation of iron oxide particles into the alginate matrix. The carbonyl vibrations of carboxylate and carboxylic acid groups and the N—H vibrations of amines and protonated amines occurred in the 1400–1750 cm^{-1} range [26], and can be used for discriminating the different states of protonation of alginate before and after the interaction with iron oxide nanoparticles. The position, width, and the intensity of FTIR peaks provided qualitative insights into the effect of the physical or chemical interactions/binding with alginate. However, quantification of the individual component from the FTIR results was difficult when the vibrational bands overlap as observed in this and other related studies [26]. The typical absorption bands at 3600–3200 cm^{-1} of alginate, assigned to the OH stretching vibrations [26], are higher in the plasticized samples, which contain a larger amount of contribution to this band due to the presence of glycerol, as indicated elsewhere [27]. The asymmetric and symmetric aliphatic C—H stretching bands were observed at 2940 and 2880 cm^{-1}, respectively. The bands at 1615 and 1450–1420 cm^{-1} were attributed to the asymmetric and symmetric stretching vibrations of carboxylate groups of alginate, respectively [17,26,28]. The absorption band due to the symmetric stretching vibrations of carboxylate groups of alginate shifts to lower frequencies with the addition of either nanoparticles or glycerol. The bands at 1037 and 947 cm^{-1} were attributed to the C—O stretching vibration of pyranosyl ring and the C—O stretching with contributions from C—C—H and C—O—H deformations [29]. The former band shifted towards higher frequencies as the glycerol content increased, as indicated in related works [27]. On the other hand, the band at 1710–1730 cm^{-1} that is due to symmetrical stretching vibration of carbonyl (—C═O) in —COOH groups [2] is absent in all the spectra because alginate based films were prepared in basic media. This band was assigned in some papers to carboxylate groups bonded onto the surface of Fe_3O_4 [17], and used as a proof of the presence of magnetite nanoparticles in the composite sample. On the other hand, Kondaveeti et al. [30], who synthesized hybrid beads composed of magnetite nanoparticles and alginate and incubated them in dopamine solution at pH 7.4, proposed that at this pH the magnetite particles are attracted towards alginate beads by ion–dipole interactions between deprotonated OH groups on the magnetic particles surfaces and OH groups of alginate.

The XRD patterns of plasticized and non-plasticized alginate films containing 10% iron oxide nanoparticles are shown in Fig. 3. Again the typical peaks corresponding to a crystalline phase of iron oxide, i.e. maghemite or magnetite, which crystallizes in the inverse spinel structure, can be barely seen. Besides, because maghemite is isostructural with magnetite it is difficult to rule out the formation of a second phase in the samples. Moreover, XRD patterns also show diffraction peaks coming from the alginate phase, as was also found in some related papers [31], probably in addition to signals coming from the sodium salts contained in the film

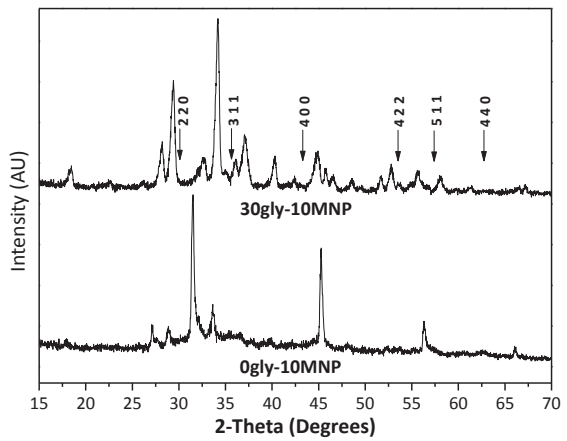

Fig. 3. XRD patterns of non-plasticized and plasticized alginate films containing 10 wt.% MNP.

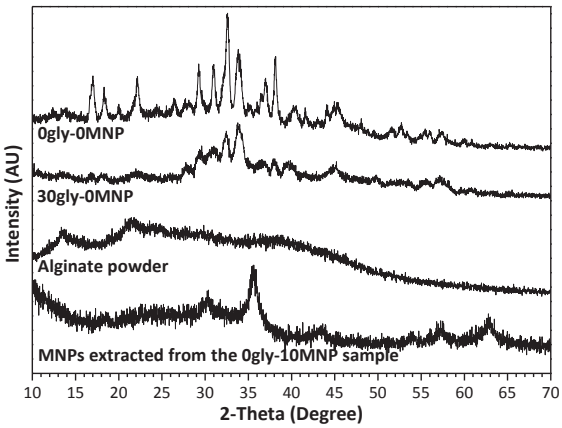

Fig. 4. XRD patterns of alginate powder, control films (without iron salts) neat and plasticized with glycerol and MNPs extracted from 0gly-10MNP sample.

forming suspensions that complicate both, the identification of the species present in the samples and the calculation of the particle size of the precipitated iron oxides by this technique. It should be taken into account that most related publications deal with iron-oxide-alginate core–shell particles or composite beads, and thus, the concentrations of iron oxide and alginate phases in the sample are similar. On the contrary, in our case the films forming suspensions were prepared to obtain a maximum nominal concentration of iron particles of 10 wt.% (i.e. 90 wt.% alginate) and accordingly, the signals coming from the magnetic phase are lower than those coming from the polymeric matrix. Thus, to further analyze this behavior, the XRD patterns of neat sodium alginate powder (raw material used to prepare the films), control films (without iron salts) neat and plasticized with glycerol and iron oxide particles extracted from the 0gly-10MNP composite film (by dissolving the film in distilled water) and deposited onto a glass surface, are presented in Fig. 4. Alginate powder exhibits two broad peaks with central positions at $2\theta = 13.5^{\circ}$ and 21.6°, respectively, which indicates two different amorphous regions, as was reported in literature [27,32]. For both alginate films (without magnetic particles), the intensity of the peak at $2\theta = 13.5^{\circ}$ decreases, indicating a lower proportion of the amorphous structure with larger chain distances as a result of the water and glycerol disruption during the processing/film forming steps. It is also noticed that for the non-plasticized alginate film, the peak at 21.6° is sharper than for the neat alginate powder due to the likely rearrangement of the alginate chains. Such phenomenon was also observed in plasticized chitosan samples obtained by thermo-mechanical mixing [27,33]. Additionally, the peak at $2\theta = 21.6^{\circ}$shifted to slightly higher angle values for the formed films. On the other hand, control films were prepared in basic media and thus they could show signals coming from NaOH crystals, being the strongest ones those appearing at $2\theta = 15.6^{\circ}$, 31.4°, 38.2°, 53.9° and 55.6°, corresponding to planes (0 2 0), (0 4 0), (1 1 1), (2 0 0) and (1 5 1), respectively [34]. However, as can be noticed from Fig. 4, the contribution of NaOH crystals solely, if any, could not explain the complex patterns found for both control films. On the other hand, the X-ray spectrum obtained from the iron oxide particles extracted from the 0gly-10MNP film shows the typical peaks corresponding to a crystalline phase of iron oxide (maghemite or magnetite) [31,35,36], which indicates clearly that the iron oxide particles were formed inside the alginate films by this simple one step co-precipitation technique, but also that the selected conditions for obtaining these materials lead to alginate films with unexpected characteristics.

Fig. 5 shows TEM images of the nanoparticles extracted from the 0gly-10MNP film at different magnifications. Some dashed circles or ovals were added on some individual particles on figures (b) and (c) to better visualize them. Due to the sample preparation method (see experimental section), the observed sizes could not be representative of all the samples. However, in the images shown it is easy to notice that the nanoparticles are less than 10 nm in all the cases. In addition, it can be noticed that not all the nanoparticles are spherical since some of them show some irregularities. Even after the intensive washing experienced by the nanoparticles after being extracted from the polymer solution, some organic phase remains on them, making it difficult to obtain better transmission electron microscopy images. This can be clearly seen on Fig. 5(a) where several nanoparticles seem to be contained on an organic phase. Fig. 5(e) shows a HT-TEM image of a selected nanoparticle from Fig. 5(d). Fast Fourier transformer (FFT) was used to quote the planes distance on the HT-TEM image (Fig. 5e) allowing to identify the (1 1 3) and (0 2 2) crystallographic planes corresponding to the Fe_3O_4 cubic space group $Fd\bar{3}m$. Summarizing, TEM analysis allowed us to confirm the formation of nanomagnetite particles with sizes in the order of 10 nm inside alginate matrix.

Selected SEM micrographs corresponding to cryo-fractured cross-sections of both unreinforced films and selected nanocomposites are shown in Fig. 6. The presence of needle crystals with different shapes is perfectly seen in all cases, with some differences according sample composition: in the neat matrix (without glycerol, Fig. 6a, magnification = 1000×), the crystals are formed mainly on or near the surface of the films (0gly-0MNP) while they are more homogeneously distributed through the thickness in the case of samples containing 30% glycerol (30gly-0MNP, Fig. 6b). The size of the crystals is also different, being those formed in the plasticized matrix larger but more heterogeneous regarding their forms and also more randomly distributed in the surface of the film (figures not shown) than those grown in the neat matrix. Sodium alginate is a natural, water-soluble polysaccharide polymer which is not known so far to crystallize spontaneously [37]. However quite recently, Haidara et al. [37] demonstrated that the controlled drying of wetting films of the alginate aqueous solution can lead to the formation of large-scale self-assembly and crystallization structures. More recently, Feng et al. [38] showed that alginate film forming solutions prepared in a pH = 7 buffer and treated by different

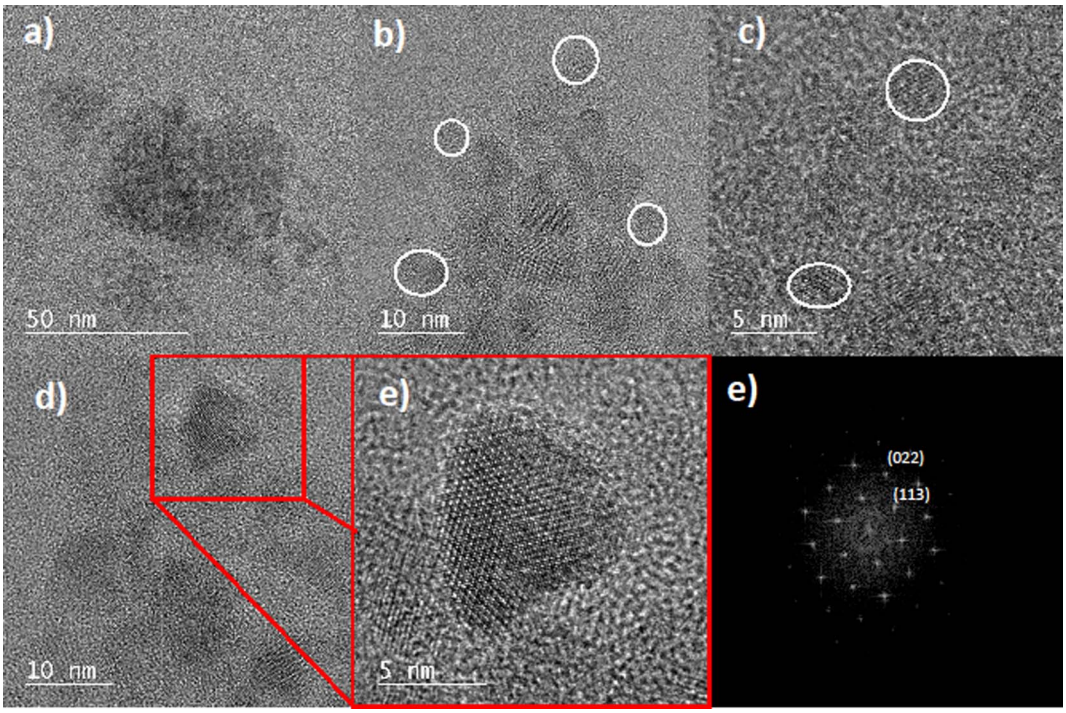

Fig. 5. (a)–(d) transmission electron microscopy at different magnification, (e) HT-TEM of selected nanoparticles of figure (d), (e) FFT of the HT-TEM on figure (d).

ultrasonic frequencies exhibited needle crystallization during drying on the silicon wafers; in some cases the needle crystals highly overlapped causing aggregation. The authors attributed this behavior to the change of interfacial activity while Hosseini et al. [39] also indicated that the sonication process promotes alginate-alginate interactions. In our case, neither controlled drying nor ultrasonication were applied to obtain the films. However, the film forming solutions were prepared in a very basic media (pH = 13–14) in contrast to what is indicated in most publications (normally prepared in distilled [40], dionized [27], ultrapure water [37] or in buffers of pH ~ 7 [38]). Hence, reports about alginate crystallization in these unusual conditions could not be found in bibliography, although the overall analysis of the results obtained from X-rays and SEM microscopies lead us to conclude that this is what is happening. Regarding composite films (Fig. 6c and d), it is interesting to notice that these crystalline structures are also present, although the concentration of crystals is lower and their size smaller (notice the magnification = 2500×) than in the corresponding matrices. This effect could be attributed to both, the lower pH of the composite film forming suspensions (the pH of the iron salts solutions is about 2 and thus, the suspensions resulting from mixing different amounts of iron salts and alginate (or alginate/glycerol) solutions have lower pH than that of the last solution) and the presence of iron oxide particles that limits crystallization of the matrix by disturbing the regularity of the structure.

Fig. 7 shows SEM micrographs of the cross sections of composite films that were obtained at higher magnification (× 10,000) in order to observe zones without crystals. The analysis of the composite samples is even more difficult due to possible presence of different inorganic salts, alginate crystals and iron oxide nanoparticles since all these inputs might contribute in different ways to increase the irregularity and roughness of the fractured cross-sections, effects that in other cases would be attributed solely to the presence of magnetic nanoparticles. Moreover, both Fe^{2+} and Fe^{3+} cations could induce cross-linkage of the alginate phase [40–42] and thus, the microstructure of the composites could differ even more from that found from the polymeric matrices. However, this effect, if present, is not significant (i.e. very low cross-linking degree), since even the films containing 10 wt.% nominal iron oxides can be almost completely solubilized in water, leaving a black solid dust in the bottom of the flask. What is clear from Fig. 6 is that the fracture of the plasticized matrix (30gly-0MNP) is more ductile than the corresponding to the non-plasticized one (0gly-0MNP) that presents ripples and ridges that might contribute to increased energy dissipation during fracture. Regarding composite samples, the fracture pattern changes with iron oxide concentration, presenting complex morphologies that go from smooth fracture paths to particulate, needle or flake-like structures. In fact, a clear relationship between the structures obtained and the nanoparticles content cannot be established from SEM observations.

Table 1 summarizes the results of the tensile tests performed on the films, showing the tensile modulus (E), ultimate strength (σ_u), ultimate deformation (ε_u) and toughness (calculated as the area under the stress–strain curve) for all samples. As expected, the addition of glycerol to the film forming solutions leads to a significant decrease in tensile stress and Young's modulus, in perfect agreement with results from related studies [27]. Regarding the elongation at break, different trends were observed. First, the plasticized matrix (without MNP) showed decreased elongation in comparison with its non-plasticized counterpart, which is quite unexpected. According to Gao et al. [27] the decreased elongation for samples with high glycerol content might be due to segregation/exudation phenomena with a significant reduction of intermolecular and intramolecular bonding in the alginate network.

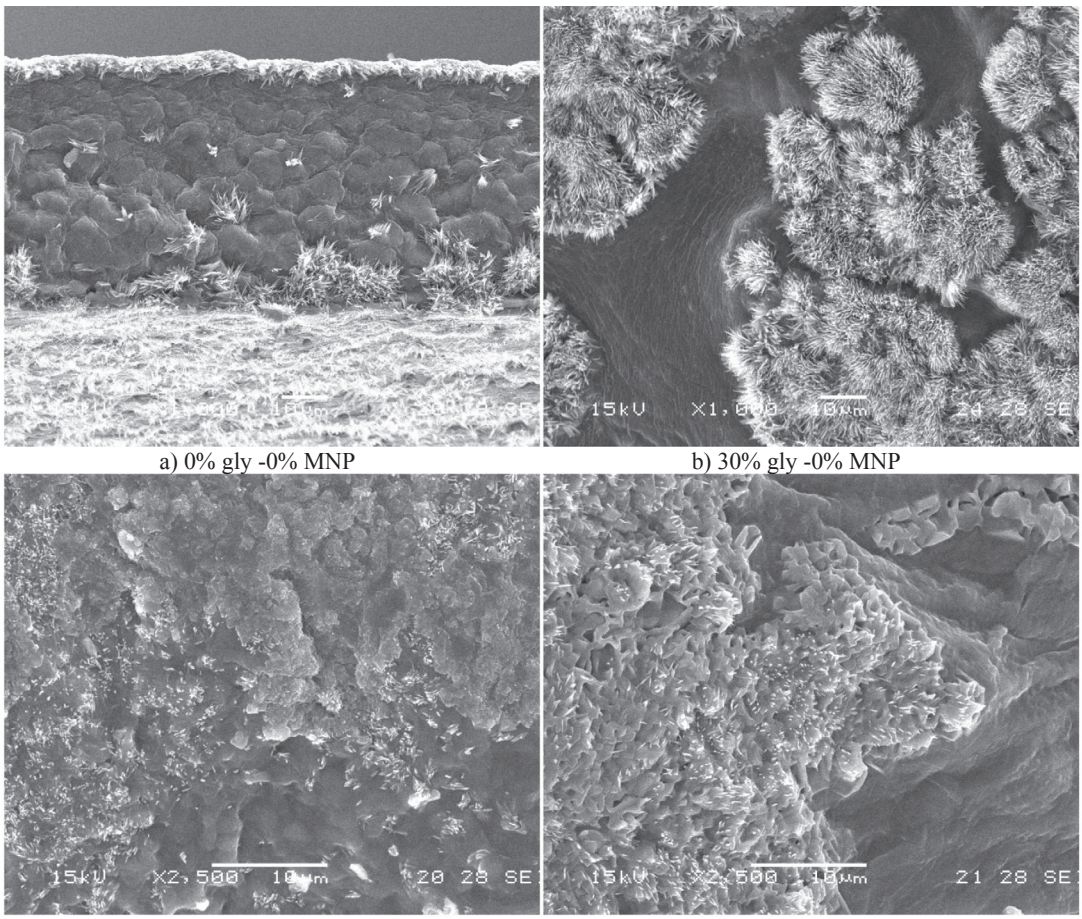

a) 0% gly -0% MNP b) 30% gly -0% MNP

c) 0% gly -10% MNP d) 30% gly -7% MNP

Fig. 6. SEM micrographs of cryo-fractured cross-sections of neat and plasticized matrices and selected nanocomposite films.

Since in our case no exudation of glycerol from plasticized films was observed, the segregation or phase separation in glycerol-rich and alginate-rich domains, as was found in chitosan based systems [43] could explain the observed behavior. But also the formation of alginate crystalline structures that lead to the obtaining of a kind of "in situ composite" (i.e. alginate matrix reinforced with alginate crystals) should be considered as a factor that influences the mechanical behavior. On the other hand, the tensile modulus of the composite films decreases as the MNP concentration increases. The ultimate strength and deformation reach a maximum for the film with 0 wt.% of MNP and 0% wt.% glycerol. This behavior could be attributed to the interactions developed between negatively charged magnetic nanoparticles (since they were prepared by in situ co-precipitation in basic media) with the negative charged carboxylate functions of alginate that reduced polymer–polymer interactions and thus, weaken the film tensile response. According to Xu et al. [2] positively charged Fe_3O_4 changed to be neutrally or negatively charged with the increasing pH levels, which rendered the interactions between nanoparticles and alginate changing from attraction to repulsion. The results for the plasticized films show a similar trend, but with reduced values of modulus and tensile strength. As an effective plasticizer, the low Mw of glycerol increases the interchain spacing and reduces interchain interactions of polysaccharides [44], favoring in particular the reduction of intermolecular and intramolecular hydrogen bonding in the alginate network [45], which leads to films with lower mechanical strength. In this sense it was quite unexpected to notice that glycerol and MNPs cause the same effect on the mechanical behavior of the composites. Regarding the deformation at break of composites, they showed similar values (if the standard deviation of the measurements is taken into account), becoming only a function of the magnetic particles concentration and independent of the glycerol content: films with 2% MNP present the lowest deformation values while for higher content of magnetic particles, film deformability increases with filler concentration. Again this behavior is believed to be due to the complex morphology developed by the samples prepared from basic film forming suspensions. Regarding toughness, unreinforced matrices exhibit higher values than composites and non-plasticized samples present higher values than plasticized ones, as the result of the combination of the different factors discussed previously.

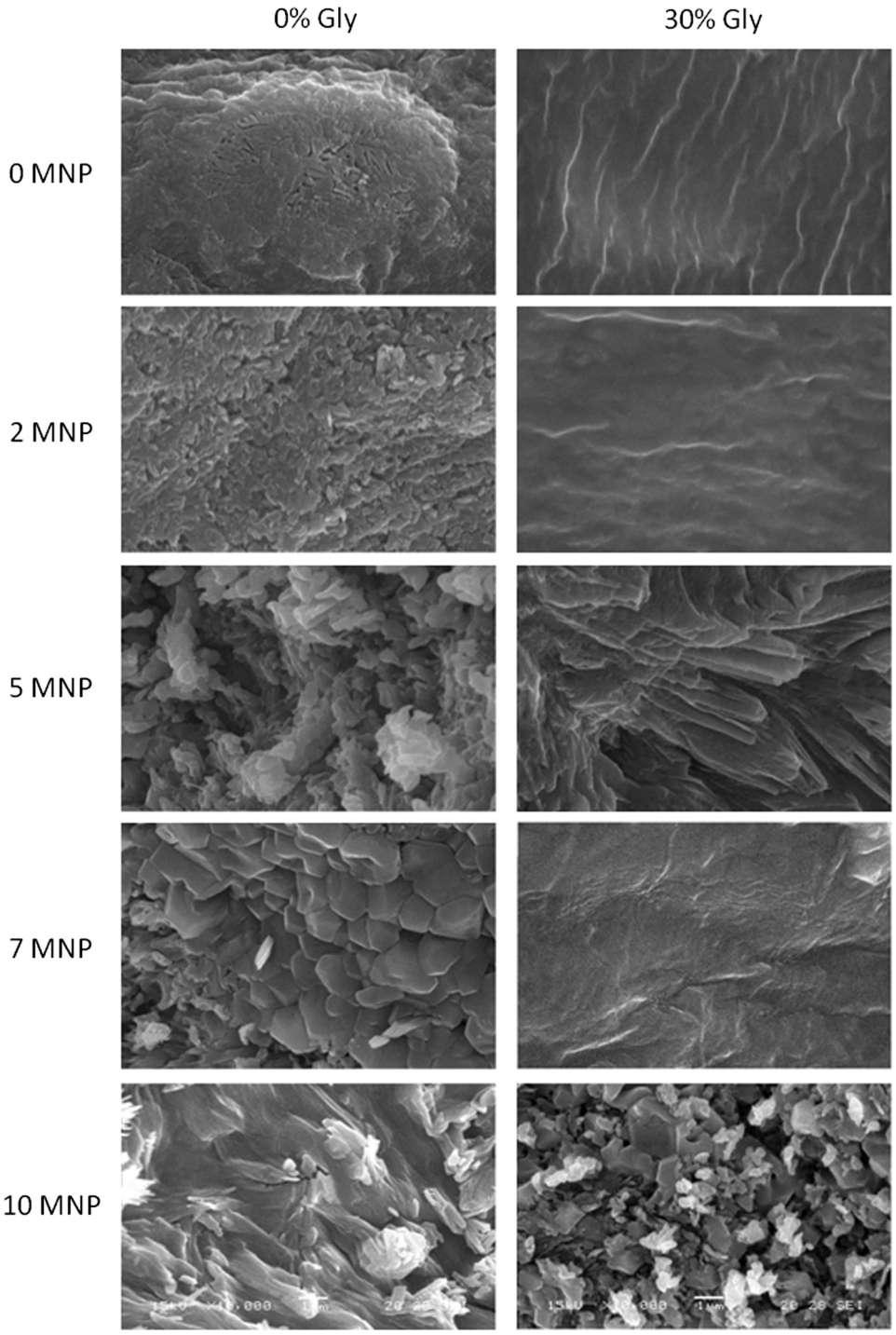

Fig. 7. SEM micrographs of the nanocomposite cross-sections as a function of the magnetic nanoparticles and glycerol concentrations. Magnification = 10,000×.

3.2. Magnetic behavior of the nanocomposite films

Composite materials have at least two contributions that define their magnetic properties. The polymeric matrix is diamagnetic, which means that under the influence of an external magnetic field, the material magnetizes in opposition to it, i.e., has a negative magnetic susceptibility. Iron oxide nanoparticles have ferromagnetic properties, but when the particle size is small enough, the energy for domains formation is larger than the one need for the formation of a monodomain. The magnetic moments on the particles rotate coherently (as a unique magnetic moment) with an applied field and hence the nanoparticles can be considered as if they had a

Table 1
Tensile properties of nanocomposite films.

Nominal MNP content (%)	Glycerol content (wt.%)	E (MPa)	σ_u (MPa)	ε_u (%)	Toughness (MPa)
0	0	673 ± 321	20.0 ± 3.5	22.1 ± 2.9	2.64 ± 0.30
2		528 ± 159	13.6 ± 2.9	6.9 ± 2.3	0.52 ± 0.33
5		232 ± 60	8.7 ± 1.0	12.3 ± 1.7	0.64 ± 0.12
7		165 ± 28	9.5 ± 1.4	13.4 ± 2.2	0.73 ± 0.19
10		216 ± 20	12.8 ± 1.3	15.2 ± 1.1	1.04 ± 0.07
0	30	113 ± 9	6.3 ± 0.6	11.9 ± 1.5	0.45 ± 0.10
2		107 ± 12	5.1 ± 0.4	7.6 ± 1.1	0.16 ± 0.03
5		48 ± 5	2.4 ± 0.1	10.1 ± 0.2	0.10 ± 0.02
7		39 ± 3	3.3 ± 0.5	14.1 ± 1.8	0.25 ± 0.06
10		25 ± 3	2.3 ± 0.7	14.8 ± 5.0	0.17 ± 0.10

single “super” magnetic moment. When the particles are a monodomain can present super-paramagnetic or ferromagnetic (also named blocked regime) behavior with positive magnetic susceptibility. The super-paramagnetic or blocked behavior is related to the size of the particles (i.e. should be below a critical size, which is ~25 nm for magnetite particles [43]) but also depends on the measurement time (τ_m), in comparison with the relaxation time (τ) of the system. When $\tau_m \gg \tau$, the nanoparticles behave like a paramagnetic material, with no hysteresis and high (super) magnetic moment. This is because the relaxation occurs faster allowing the system to reach thermodynamic equilibrium. Because τ is also temperature dependant, according to Néel-Arrhenius law ($\tau = \tau_0 \exp(K_a V_0/k_B T)$, where τ_0 is a pre-exponential factor, K_a is the anisotropy energy density, V_0 is the magnetic volume of the nanoparticles, and k_B is the Boltzmann constant) for a specific τ_m, and varying the temperature is possible to crossover from blocked regime (lower temperature) to super-paramagnetic regime (higher temperature). If the temperature is low enough, τ_m will be shorter than the average relaxation time and the system will be on the blocked regime. As the temperature increases, for certain temperatures τ_m will be larger than the average relaxation time and the system will be on the super-paramagnetic regime. The blocking temperature (T_B) is the temperature that for a fixed τ_m separates the blocked regime from the paramagnetic one. At this temperature $\tau_m = \tau$, i.e. the temperature above which the thermal energy overcomes the energy barrier related to the change in the orientation of the magnetic moment [46–48]. The T_B for a SQUID-Magnetometer measurement can be derived directly from the Néel-Arrhenius law considering that τ_m is about 100 s [49] being:

$$T_B \approx \frac{K_a V_0}{25 * k_B},$$

therefore T_B increases with increasing particle size, anisotropy constant, or the energy barrier product $U = K_a V_0$. Above the blocking temperature the nanoparticles behave like a paramagnet with temperature dependence of the magnetization according Curie law (inverse temperature dependence of magnetic susceptibility) and a “super” magnetic moment.

To study the magnetic response of the nanocomposites, Zero Field Cooling (ZFC) – Field Cooling (FC) magnetization tests were made. The curves obtained are display in Fig. 8. All the films present a maximum in the ZFC curve, which is taken as the T_B and shown in Table 2 as a function of nanoparticle concentration. It can be seen that the non-plasticized films exhibit higher T_B than the plasticized ones. For both series (with and without glycerol), T_B increases as the MNP content in the films increases. According to the last equation, the increase in T_B could be due to an increment in the size of the particles or to the formation of agglomerates, which act as larger energy barrier, *U*. Since TEM observations from nanomagnetite particles extracted from the 0gly-10MNP film indicate that their individual size is less than 10 nm, this behavior should be related with the formation of agglomerates of larger size in the non-plasticized alginate matrices as compared with the alginate-glycerol matrix, probably due to the higher difficulty of the particles to disperse themselves in these more rigid (in comparison with plasticized ones) films. However, there are also other factors that should be taken into account, for example we found in a previous work [43] that the size of the precipitated MNP is strongly influenced by the phase where it grows. Moreover, the interaction between the polymer and the iron ions could be explained by a site-binding model [6]. The low Mw of glycerol favours the reduction on intermolecular and intramolecular hydrogen bonding in the alginate network [45], allowing in this case the formation of a larger number of centres of nucleation for the iron oxide particles that, according to the results presented in Table 2, grow less than in the non-plasticized alginate matrix.

On the other hand, evidently the negatively charged magnetite particles prefer to interact with other particles instead of being surrounded by the negatively charged alginate molecules when there is no plasticizer in the film forming solution. Mascolo et al. [36] indicated that several factors including the alkali selected for the precipitation of nanomagnetite, pH of the solution, reaction temperature, concentration of precursors and slow or fast mixing of reagents are known to control the nucleation and growth of the magnetite nanoparticles and can influence the magnetite properties, e.g., particle size and saturation magnetization (Ms). In this work, the concentration of precursors of the film forming solution for plasticized or non-plasticized films were different (lower concentrations for the glycerol containing solutions since the iron oxide precursors concentration was based on neat alginate, instead of alginate + glycerol, weight). Moreover, the pH of the suspensions leading to the different concentrations of iron oxides are different, as indicated previously. Thus, these factors could also contribute to define the number as well as the final size of the nanoparticles/agglomerates formed in both polymeric matrices. Moreover, the magnetic behavior of the material is strongly influenced by nanoparticle agglomerates in which inner particles display inter-particle interactions and only those located in the external

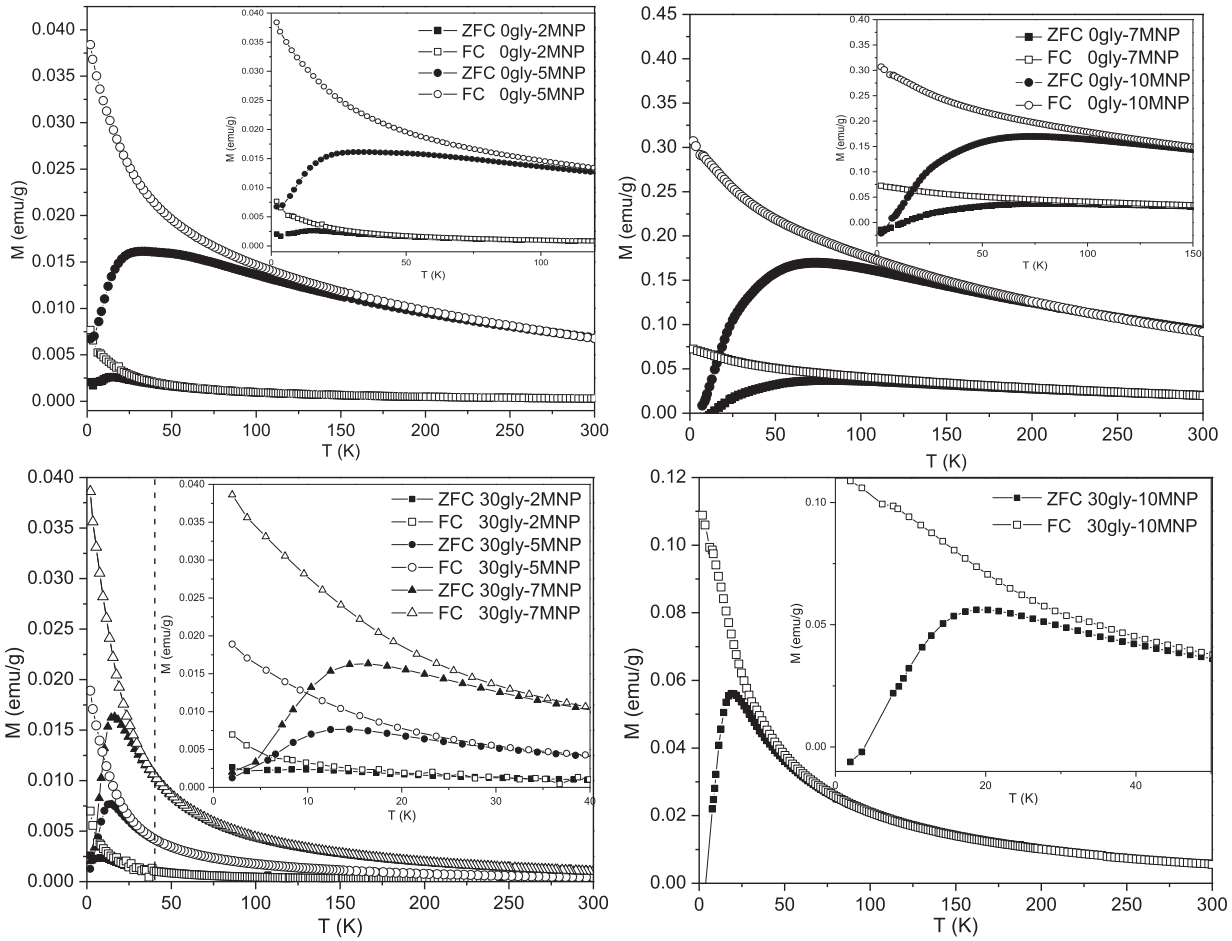

Fig. 8. Zero Field Cooling/Field Cooling measurements for the non-plasticized and plasticized films.

Table 2
T_B and T_i obtained from the ZFC-FC tests.

Nominal MNP content (%)	Glycerol content (wt.%)	T_B (K)	T_i (K)
2	0	15.8	50
5		34.4	130
7		80.4	155
10		72.6	190
2	30	8.3	30
5		14.4	40
7		16.4	45
10		18.8	50

shell of the agglomerate can interact with the polymeric matrix or with other magnetic particles/agglomerates.

The irreversibility temperature (T_i) is the temperature where the difference between the ZFC and FC ($(dM_{FC}\text{-}dM_{ZFC})/dT$) curves is less than 10 %. The differences between T_B and T_i are indicative of the size/anisotropy distribution and dipolar interaction between the nanoparticles. When T_B and T_i are the same, there is a narrow particle size/anisotropy distribution and absence of magnetic dipolar interaction between the nanoparticles [50]. As we can see in Table 2, for all the non-plasticized films T_i and T_B are very different, corresponding to polydispersed systems or strong interaction between the nanoparticles. For the plasticized samples T_i and T_B are closer, which correspond to a relatively narrow size distribution of particles and low interactions between them. Also from ZFC measurements for temperatures higher than T_B it can be noticed that the plasticized samples show a Curie type behavior whereas the non-plasticized films are apart from this, confirming the existence of interaction between the nanoparticles in the last case.

To complement the ZFC-FC analysis, the isothermal magnetization (M) as a function of the applied magnetic field (H) was measured at 2 K and 300 K. Fig. 9a-b shows isothermal curves of magnetization (M) versus applied magnetic field (H) for non-plasticized films at two different iron oxide compositions (5 and 10 wt.% MNP) at 2 and 300 K. At 2 K, both curves confirm the

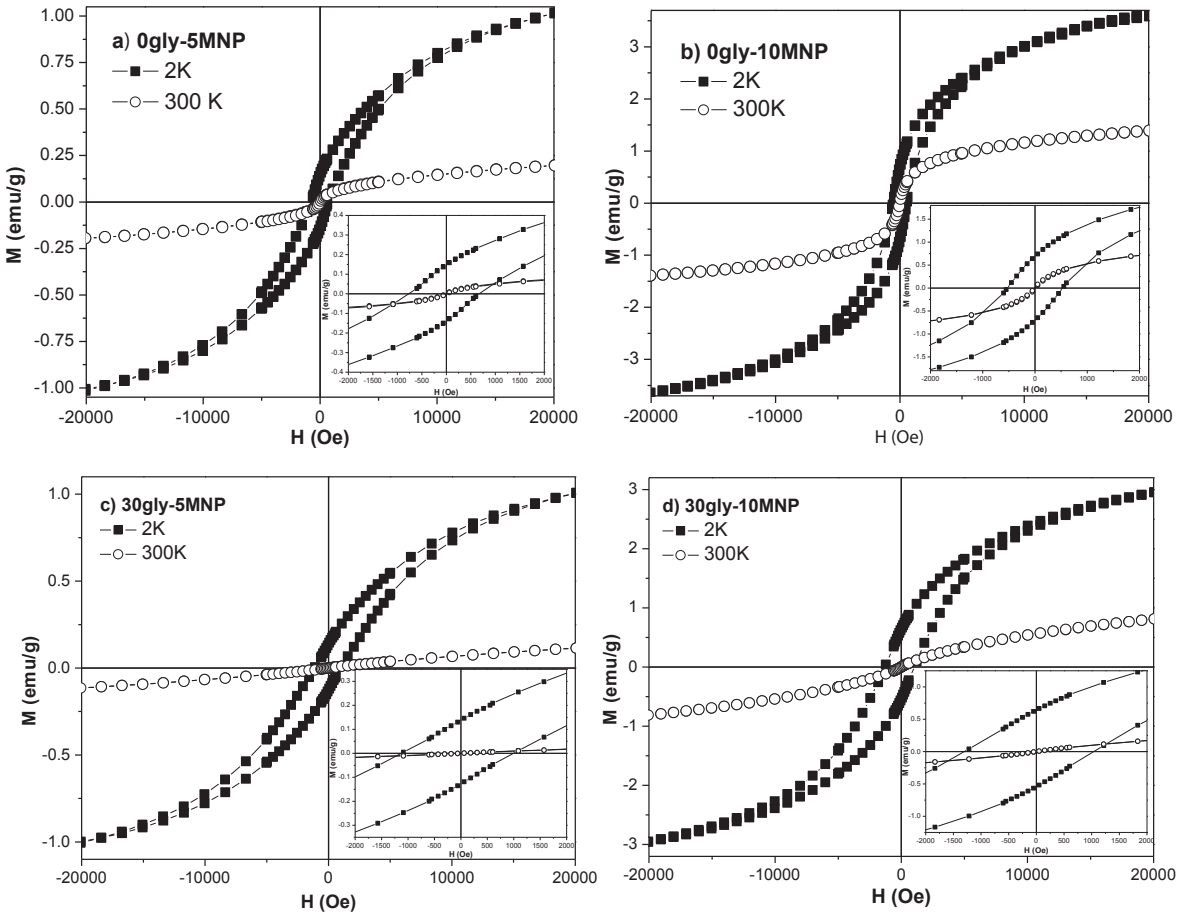

Fig. 9. Magnetization (M) vs applied field (H) curves at 2 K and 300 K for non-plasticized samples containing 5 (a) and 10 wt.% MNP (b) and plasticized samples containing 5 (c) and 10 wt.% MNP (d).

blocked regime due to the presence of hysteresis, as it was mentioned before. The obtained coercive fields at 2 K are summarized in Table 3. At 300 K the measurements showed typical super-paramagnetic behavior with no hysteresis when the isothermal tests are performed. The results of the curves at 300 K show zero or negligible coercive field. The magnetization at high field (± 20 kOe) value decreases as the temperature increases, which is consistent with the superparamagnetic regime at 300 K in comparison with the blocked state at 2 K. As the content of nanoparticles increases, M (H = ± 20 kOe) also increases due to the increased amount of magnetic material in the sample. Even so, for all the tested samples and in concordance to what literature mentioned for some types of magnetic nanocomposites, the values of magnetization at high fields are very small in comparison with the value of the bulk of magnetite [36,51–54]. It is also important to remark that the results shown in Fig. 9 and Table 3 denote that the values of M at 20 KOe are far to be the saturation magnetization. This fact could be associated to the paramagnetic contribution due to the presence of Fe (II) and Fe (III) (from the iron salts solutions used at the initial step of the composite preparation) that could not precipitate into iron oxides and thus would decrease the percentage of particles with magnetic properties into the films, and also to the effect of

Table 3
Magnetization (M) at H = 20 kOe and coercitivy fields (Hc) at 2 and 300 K.

Nominal MNP content (%)	Glycerol content (wt. %)	M(H = ± 20 kOe) at 2 K (emu/g)	M (H = ± 20 kOe) at 300 K (emu/g)	Hc at 2 K (Oe)	Hc at 300 K (Oe)
2	0	0.68	0.03	514	50
5		1.02	0.10	670	6
7		–	0.47	–	7
10		3.61	1.39	526	10
2	30	0.80	0.0245	365	49
5		1.01	0.11	1000	10
7		2.04	0.265	1005	6
10		2.95	0.81	1037	11

others salts like NaCl and Na_2SO_4 formed during the film synthesis (as was indicated previously). Moreover, the presence of glycerol provokes a significant increase in the coercive filed at low temperature (2 K) because of changes in the anisotropy distribution, as can be noticed from Fig. 9c–d and Table 3.

4. Conclusions

Magnetic nanocomposite plasticized and non-plasticized films based on alginate and iron oxide particles with different amounts of nanoparticles precipitated "in situ" were successfully obtained. The way of synthesis was a simple one step in situ co-precipitation method, followed by solvent-casting. However, the understanding of the final response of these systems resulted more complex than expected due to the presence of plasticizer, residual salts and ions, crystalline regions attributed to alginate crystallization and repulsive interactions developed between both negatively charged phases (alginate and iron oxide particles). Any of these factors affected in different ways the final properties of the composite films, i.e. the X-ray patterns and FTIR spectra of composite samples did not allow us to identify the iron oxide/s formed but the former revealed polymer crystallization, which was further confirmed by SEM micrographs. The decrease of the modulus and tensile strength with particle concentration was mainly attributed to both the glycerol content in the films but also to the repulsion between particles and matrix. Moreover, size of the magnetic particles/agglomerates formed in the films depended strongly on the concentration of iron precursors and glycerol, as was inferred from the measured magnetic properties. The larger and more polydisperse magnetic particles/agglomerates were formed in the non-plasticized films while relatively small, separated particles grew in the plasticized ones. All the films containing iron oxide particles presented super paramagnetic behavior, which ensures that they could be recovered by using a magneto after used in an adsorption process. Nevertheless, we can infer that the plasticized samples reproduce the magnetic behavior of a system nearer the ideal well dispersed super-paramagnetic one than the non-plasticized films.

Acknowledgements

The authors acknowledge the financial support provided by the National Research Council of Argentina (CONICET, Grant PIP 0637), the Science and Technology National Promotion Agency (ANPCyT, Grant PICT-2013-1535) and the National University of Mar del Plata – Argentina (Project # 15/G430). The work at UNICAMP was supported by FAPESP (2011/1234-6) Brazil. We also like to acknowledge Prof. K. R. Pirota and Prof. M. Knobel for allowing us to use the SQUID magnetometer at LMBT/IFGW/UNICAMP and also the C2NANO-Brazilian Nanotechnology National Laboratory (LNNano) at Centro Nacional de Pesquisa em Energìa e Materiais CNPEM/MCT (#19927) for taking the TEM images.

References

[1] D.H.K. Reddy, S.M. Lee, Application of magnetic chitosan composites for the removal of toxic metal and dyes from aqueous solutions, Adv. Colloid Interface Sci. 201–202 (2013) 68–93.
[2] X.Q. Xu, H. Shen, J.R. Xu, M.Q. Xie, X.J. Li, The colloidal stability and core-shell structure of magnetite nanoparticles coated with alginate, Appl. Surf. Sci. 253 (2006) 2158–2164.
[3] M.M. Lakouraj, F. Mojerlou, E.N. Zare, Nanogel and superparamagnetic nanocomposite based on sodium alginate for sorption of heavy metal ions, Carbohydr. Polym. 106 (2014) 34–41.
[4] T. Salomonsen, H.M. Jensen, D. Stenbæk, S.B. Engelsen, Chemometric prediction of alginate monomer composition: a comparative spectroscopic study using IR, Raman, NIR and NMR, Carbohydr. Polym. 72 (2008) 730–739.
[5] Y. Nishio, A. Yamada, K. Ezaki, Y. Miyashita, H. Furukawa, K. Horie, Preparation and magnetometric characterization of iron oxide-containing alginate/poly (vinyl alcohol) networks, Polymer (Guildf) 45 (2004) 7129–7136.
[6] H. Ma, X. Qi, Y. Maitani, T. Nagai, Preparation and characterization of superparamagnetic iron oxide nanoparticles stabilized by alginate, Int. J. Pharm. 333 (2007) 177–186.
[7] K.J. Sreeram, H.Y. Shrivastava, B.U. Nair, Studies on the nature of interaction of iron(III) with alginates, Biochim. Biophys. Acta – Gen. Subj. 1670 (2004) 121–125.
[8] R. Karthik, S. Meenakshi, Removal of Cr(VI) ions by adsorption onto sodium alginate-polyaniline nanofibers, Int. J. Biol. Macromol. 72 (2015) 711–717.
[9] K. Yu, J. Ho, E. McCandlish, B. Buckley, R. Patel, Z. Li, N.C. Shapley, Copper ion adsorption by chitosan nanoparticles and alginate microparticles for water purification applications, Colloids Surf. A Physicochem. Eng. Asp. 425 (2013) 31–41.
[10] W. Jung, B.-H. Jeon, D.-W. Cho, H.-S. Roh, Y. Cho, S.-J. Kim, D.S. Lee, Sorptive removal of heavy metals with nano-sized carbon immobilized alginate beads, J. Ind. Eng. Chem. 26 (2014) 364–369.
[11] Y. Konishi, S. Asai, Y. Midoh, M. Oku, Recovery of zinc, cadmium, and lanthanum by biopolymer gel particles of alginic acid, Sep. Sci. Technol. 28 (1993) 1691–1702.
[12] K.J. Sreeram, M. Nidhin, B.U. Nair, Synthesis of aligned hematite nanoparticles on chitosan-alginate films, Colloids Surfaces B Biointerfaces. 71 (2009) 260–267.
[13] H. Pardoe, W. Chua-anusorn, T.G. St Pierre, J. Dobson, Structural and magnetic properties of nanoscale iron oxide particles synthesized in the presence of dextran or polyvinyl alcohol, J. Magn. Magn. Mater. 225 (2001) 41–46.
[14] E. Kroll, F.M. Winnik, R.F. Ziolo, In situ preparation of nanocrystalline γ-Fe_2O_3 in iron(II) cross-linked alginate gels, Chem. Mater. 8 (1996) 1594–1596.
[15] F. Llanes, D.H. Ryan, R.H. Marchessault, Magnetic nanostructured composites using alginates of different M/G ratios as polymeric matrix, Int. J. Biol. Macromol. 27 (2000) 35–40.
[16] F. Shen, C. Poncet-Legrand, S. Somers, A. Slade, C. Yip, A.M. Duft, F.M. Winnik, P.L. Chang, Properties of a novel magnetized alginate for magnetic resonance imaging, Biotechnol. Bioeng. 83 (2003) 282–292.
[17] A. Mohammadi, H. Daemi, M. Barikani, Fast removal of malachite green dye using novel superparamagnetic sodium alginate-coated Fe_3O_4 nanoparticles, Int. J. Biol. Macromolec. 69 (2014) 447–455.
[18] A.E. Regazzoni, G.A. Urrutia, M.A. Blesa, A.J.G. Maroto, Some observations on the composition and morphology of synthetic magnetites obtained by different routes, J. Inorg. Nucl. Chem. 43 (1981) 1489–1493.
[19] D.J. Shaw, Introduction to Colloid and Surface Chemistry, fourth ed., Butterworth Heinemann (a division of Reed Educational and Professional Publishers), Woburn, 1992
[20] G.A. Kloster, N.E. Marcovich, M.A. Mosiewicki, Composite films based on chitosan and nanomagnetite, Eur. Polym. J. 66 (2015) 386–396.

[21] V. Belessi, R. Zboril, J. Tucek, M. Mashlan, V. Tzitzios, D. Petridis, Ferrofluids from magnetic-chitosan hybrids, Chem. Mater. 20 (2008) 3298–3305.
[22] V.L. Lassalle, R.D. Zysler, M.L. Ferreira, Novel and facile synthesis of magnetic composites by a modified co-precipitation method, Mater. Chem. Phys. 130 (2011) 624–634.
[23] S. Ben Hammouda, N. Adhoum, L. Monser, Synthesis of magnetic alginate beads based on Fe_3O_4nanoparticles for the removal of 3-methylindole from aqueous solution using Fenton process, J. Hazard. Mater. 294 (2015) 128–136.
[24] S. Li, T. Zhang, R. Tang, H. Qiu, C. Wang, Z. Zhou, Solvothermal synthesis and characterization of monodisperse superparamagnetic iron oxide nanoparticles, J. Magn. Magn. Mater. 379 (2015) 226–231.
[25] X.N. Pham, T.P. Nguyen, T.N. Pham, T.T.N. Tran, T.V.T. Tran, Synthesis and characterization of chitosan-coated magnetite nanoparticles and their application in curcumin drug delivery, Adv. Nat. Sci. Nanosci. Nanotechnol. 7 (2016) 45010.
[26] De Long-Feng Wang, Shiv Shankar, Jong-Whan Rhim, Properties of alginate-based films reinforced with cellulose fibers and cellulose nanowhiskers isolated from mulberry pulp, Food Hydrocoll. 63 (2017) 201–208.
[27] C. Gao, E. Pollet, L. Avérous, Properties of glycerol-plasticized alginate films obtained by thermo-mechanical mixing, Food Hydrocoll. 63 (2017) 414–420.
[28] Q. Xiao, X. Gu, S. Tan, Drying process of sodium alginate films studied by two-dimensional correlation ATR-FTIR spectroscopy, Food Chem. 164 (2014) 179–
[29] H. Daemi, M. Barikani, M. Barmar, Compatible compositions based on aqueous polyurethane dispersions and sodium alginate, Carbohydr. Polym. 92 (2013) 490–496.
[30] S. Kondaveeti, D.R. Cornejo, D. Freitas Siqueira Petri, Alginate/magnetite hybrid beads for magnetically stimulated release of dopamine, Colloids Surfaces B Biointerfaces 138 (2016) 94–101.
[31] M.A. Morales, P.V. Finotelli, J.A.H. Coaquira, M.H.M. Rocha-Leão, C. Diaz-Aguila, E.M. Baggio-Saitovitch, A.M. Rossi, In situ synthesis and magnetic studies of iron oxide nanoparticles in calcium-alginate matrix for biomedical applications, Mater. Sci. Eng. C. 28 (2008) 253–257.
[32] V. Paşcalau, V. Popescu, G.L. Popescu, M.C. Dudescu, G. Borodi, A. Dinescu, I. Perhaiţa, M. Paul, The alginate/k-carrageenan ratio's influence on the properties of the cross-linked composite films, J. Alloys Compd. 536 (2012) 418–423.
[33] M. Matet, M.C. Heuzey, E. Pollet, A. Ajji, L. Avérous, Innovative thermoplastic chitosan obtained by thermo-mechanical mixing with polyol plasticizers, Carbohydr. Polym. 95 (2013) 241–251, http://dx.doi.org/10.1016/j.carbpol.2013.02.052.
[34] International Centre for Diffraction Data, PDF-2 (2004), file N°00-001-1173.
[35] M. Srivastava, J. Singh, M. Yashpal, D.K. Gupta, R.K. Mishra, S. Tripathi, A.K. Ojha, Synthesis of superparamagnetic bare Fe_3O_4 nanostructures and core/shell (Fe_3O_4/alginate) nanocomposites, Carbohydr. Polym. 89 (2012) 821–829.
[36] M.C. Mascolo, Y. Pei, T.A. Ring, Room temperature co-precipitation synthesis of magnetite nanoparticles in a large pH window with different bases, Materials 6 (2013) 5549–5567.
[37] H. Haidara, L. Vonna, L. Vidal, Unrevealed self-assembly and crystallization structures of Na-alginate, induced by the drying dynamics of wetting films of the aqueous polymer solution, Macromolecules 43 (2010) 2421–2429.
[38] L. Feng, Y. Cao, D. Xu, S. Wang, J. Zhang, Molecular weight distribution, rheological property and structural changes of sodium alginate induced by ultrasound, Ultrason. Sonochem. 34 (2017) 609–615.
[39] S.M. Hosseini, H. Hosseini, M.A. Mohammadifar, A.M. Mortazavian, A. Mohammadi, K. Khosravi-Darani, S. Shojaee-Aliabadi, S. Dehghan, R. Khaksar, Incorporation of essential oil in alginate microparticles by multiple emulsion/ionic gelation process, Int. J. Biol. Macromol. 62 (2013) 582–588.
[40] P. Singh, S.K. Singh, J. Bajpai, A.K. Bajpai, R.B. Shrivastava, Iron crosslinked alginate as novel nanosorbents for removal of arsenic ions and bacteriological contamination from water, J. Mater. Res. Technol. 3 (2014) 195–202.
[41] B.Y. Swamy, Y.S. Yun, In vitro release of metformin from iron (III) cross-linked alginate-carboxymethyl cellulose hydrogel beads, Int. J. Biol. Macromol. 77 (2015) 114–119.
[42] I. Machida-Sano, S. Ogawa, H. Ueda, Y. Kimura, N. Satoh, H. Namiki, Effects of composition of iron-cross-linked alginate hydrogels for cultivation of human dermal fibroblasts, Int. J. Biomater. 2012 (2012).
[43] G.A. Kloster, D. Muraca, C. Meiorin, K.R. Pirota, N.E. Marcovich, M.A. Mosiewicki, Magnetic characterization of chitosan – magnetite nanocomposite films, Eur. Polym. J. 72 (2015) 202–211.
[44] F. Hammann, M. Schmid, Determination and quantification of molecular interactions in protein films: a review (2014) 7975–7996.
[45] V. Jost, K. Kobsik, M. Schmid, K. Noller, Influence of plasticiser on the barrier, mechanical and grease resistance properties of alginate cast films, Carbohydr. Polym. 110 (2014) 309–319.
[46] D.L. Leslie-Pelecky, R.D. Rieke, Magnetic properties of nanostructured materials, Chem. Mater. 8 (1996) 1770–1783.
[47] A. Labarta, X. Batlle, O. Iglesias, From finite size and surface effects to glassy behaviour in ferrimagnetic nanoparticles, chapter 4 in the book: "Surface effects in magnetic nanoparticles", in: D. Fiorani (Ed.), Nanostructured Science and Technology Series, Springer Science + Business Inc., Nueva York, 2005.
[48] M.A. Garza-Navarro, V. González, M. Hinojosa., A. Torres Castro, Preparation of chitosan/magnetite polymeric-magnetic films, Revista Mexicana de Física 57 (2011) 51–56.
[49] B. Martínez, A. Roig, X. Obradors, E. Molins, A. Rouanet, C. Monty, Magnetic properties of γ-Fe_2O_3 nanoparticles obtained by vaporization condensation in a solar furnace, J. Appl. Phys. 79 (1996) 2580–2586.
[50] O. Moscoso-Londoño, P. Tancredi, D. Muraca, P. Mendoza Zélis, D. Coral, M.B. Fernández van Raap, U. Wolff, V. Neu, C. Damm, C.L.P. de Oliveira, K.R. Pirota, M. Knobel, L.M. Socolovsky, Different approaches to analyze the dipolar interaction effects on diluted and concentrated granular superparamagnetic systems, J. Magn. Magn. Mater. 428 (2017) 105–118.
[51] A.S. Bhatt, D. Krishna Bhat, M.S. Santosh, Electrical and magnetic properties of chitosan-magnetite nanocomposites, Phys. B Condens. Matter. 405 (2010) 2078–2082.
[52] K. Petcharoen, A. Sirivat, Synthesis and characterization of magnetite nanoparticles via the chemical co-precipitation method, Mater. Sci. Eng. B Solid-State Mater. Adv. Technol. 177 (2012) 421–427.
[53] Y. Ding, Y. Hu, L. Zhang, Y. Chen, X. Jiang, Synthesis and magnetic properties of biocompatible hybrid hollow spheres, Biomacromolecules 7 (2006) 1766–1772.
[54] K.V.P.M. Shafi, Y. Koltypin, A. Gedanken, J. Lendvai, I. Felner, Sonochemical preparation of nanosized amorphous $NiFe_2O_4$ particles, J. Phys. Chem. B. 5647 (1997) 6409–6414.